

Symmetry-driven large Tunneling Magnetoresistance in SrRuO_3 Magnetic Tunnel Junctions with Perpendicular Magnetic Anisotropy

Anouk S. Goossens,^{1, 2} Kartik Samanta,³ Azminul Jaman,^{1, 2} Wissem Boubaker,¹
Job J. L. van Rijn,¹ Evgeny Y. Tsymbal,³ and Tamalika Banerjee^{1, 2, *}

¹ *Zernike Institute for Advanced Materials
University of Groningen 9747 AG, Groningen The Netherlands*

² *Groningen Cognitive Systems and Materials Center,
University of Groningen 9747 AG, Groningen The Netherlands*

³ *Department of Physics and Astronomy & Nebraska Center for Materials and Nanoscience,
University of Nebraska, Lincoln, Nebraska 68588, USA*

(Dated: April 17, 2024)

Magnetic tunnel junctions (MTJs) that are comprised of epitaxially-grown complex oxides offer a versatile platform to control the symmetry of tunneling states and tailor magnetic anisotropy useful for practical applications. This work employs thin films of SrTiO_3 as an insulating barrier deposited between two ferromagnetic SrRuO_3 electrodes to form fully epitaxial MTJs and demonstrate these functionalities. Transport measurements demonstrate large tunneling magnetoresistance (TMR), significantly exceeding previously found values of TMR in MTJs based on SrRuO_3 electrodes. These results are explained by perpendicular magnetic anisotropy of SrRuO_3 and matching (mismatching) between symmetry and spin across the $\text{SrTiO}_3/\text{SrRuO}_3$ (001) interface for the parallel (antiparallel) MTJ magnetization state, supported by density functional (DFT) calculations. The angular variation of TMR indicates that the SrRuO_3 electrodes contain multiple magnetic domains, allowing the devices to exhibit at least three stable resistance states.

The exploration of spin-dependent tunneling in magnetic tunnel junctions (MTJs) has garnered significant interest, forming the foundation for spin-electronic devices like hard disk drives and magnetoresistive random access memories (MRAMs). MTJs remain the most widely investigated device structure in spintronics, characterized by their relatively straightforward structure, and electronic properties that depend on the choice of ferromagnetic and tunnel barrier layers. In the simplest model of tunneling magnetoresistance (TMR), the magnitude depends exclusively on the tunnel spin polarization of the density of states (DOS) at the Fermi energy, E_F of the two ferromagnets, which was initially considered to be an intrinsic property of the ferromagnet. It has, however, been shown that the transmission probability depends on the barrier itself and both the nature of evanescent states within the barrier as well as bonding at the ferromagnet/barrier affect TMR[1–4]. The nature of the bonding, for instance, can result in either positive or negative tunnel spin polarization[5, 6] and hence it should be considered as the product of the transmission matrix at ferromagnet-barrier interfaces rather than of the ferromagnet alone.

The introduction of MgO marked a turning point, as it provided a spin-dependent match between the evanescent states in the tunnel barrier and the electronic states of the electrodes, resulting in high TMR ratios[1, 7]. Additionally, interfacial anisotropy between MgO and the ferromagnet can promote perpendicular magnetic anisotropy (PMA)[8] making MgO one of the most widely used tunnel barriers for MTJs. Recently, a record room temperature TMR ratio of 631% was reported

in $\text{CoFe}/\text{MgO}/\text{CoFe}$ MTJs[9]. Epitaxial interfaces in MTJs have opened important avenues for studying spin-polarized tunneling, facilitating the exploration of magnetization and anisotropy effects with applications in MRAM, neuromorphic, and probabilistic computing[10–12]. The close lattice match and chemical compatibility between these materials enable the growth of heterostructures with high-quality interfaces, which is important for realizing spin-polarized tunneling.

Complex oxides are an important material class endowed with a rich phase space and exploiting strong correlation effects and topology. Their versatility in creating epitaxial interfaces, utilizing strain control, designing crystalline symmetry, and tailoring spin-orbit coupling effects, is less explored but essential for the development of a new generation of MTJs with enhanced functionalities and performance. Using SrTiO_3 (STO) as a tunnel barrier, for example, a TMR of 1800% was demonstrated in $\text{LSMO}/\text{STO}/\text{LSMO}$ MTJs[13]. The existence of d-orbitals in both the tunnel barrier as well as the electrodes in these complex oxide systems plays an important role. The complex band structure of STO is formed from localized 3d states of Ti, which allows efficient tunneling of d electrons[4]. Using first-principles calculations it was shown that tunneling across SrRuO_3 (SRO)/ BaTiO_3 interfaces gives rise to a correspondence between symmetry and spin due to the preservation of wave function symmetry resulting in high TMR ratios up to 75%[14]. MTJs utilizing electrodes with perpendicular magnetic anisotropy are of great interest for future non-volatile memory and logic chips with high thermal stability and packing densities. To attain PMA, however,

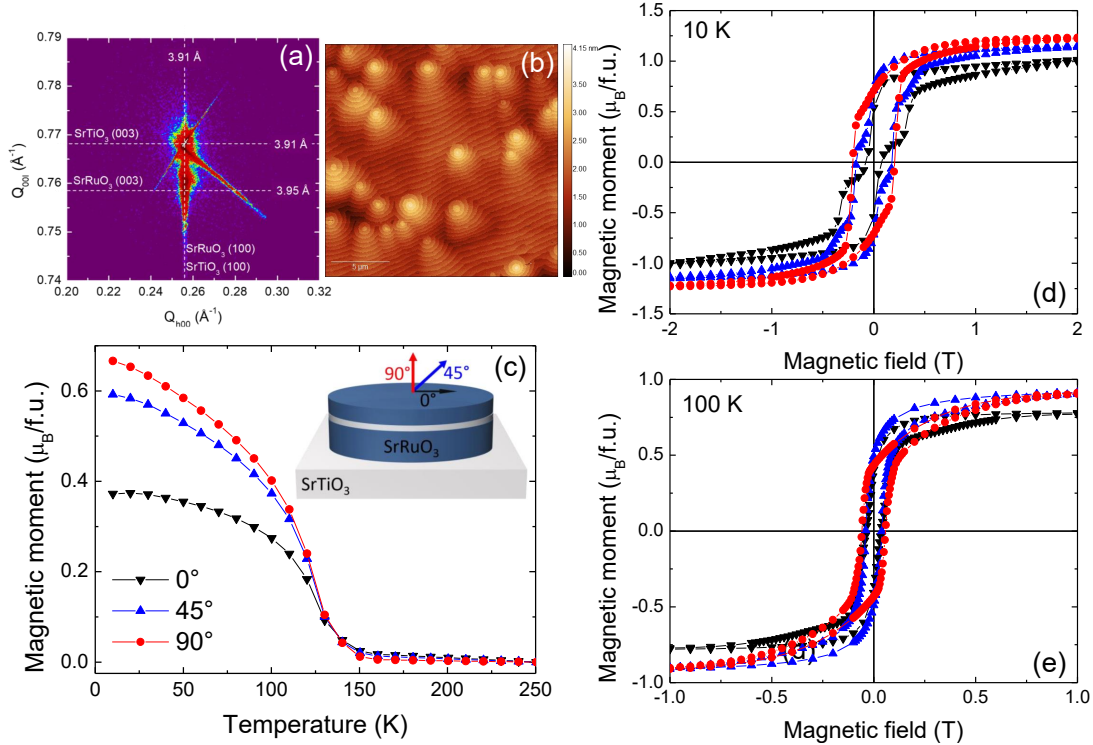


FIG. 1. Characterization of stacks after pulsed laser deposition. (a) Reciprocal space maps around the (103) peaks. (b) Atomic force microscopy image of top surface. (c) 6.5 T field cooled magnetization versus temperature. Magnetization versus magnetic field at (d) 10 K and (e) 100 K. In (c)-(e) the magnetic field is applied in the plane of the film (black triangles), 45° to the normal (blue triangles) and normal to the film (red circles).

typically complex stacks are required for MTJs[15, 16].

The work presented here focuses on all-oxide MTJs using STO as the insulating barrier and SRO layers of varying thicknesses as ferromagnetic metallic electrodes. SRO is an itinerant ferromagnet with a bulk Curie temperature of 160 K [17] where the magnetism is driven by Ru 4d electrons[18]. SRO has been extensively investigated and many interesting magnetic phenomena, such as topological Hall effects, Weyl fermions and topological textures, e.g. skyrmion bubbles, were reported[19–25]. SRO thin films exhibit PMA that can be tailored by the substrate. For example, due to the close lattice match to STO, SRO films can be grown with either perfectly perpendicular anisotropy (PMA) on STO (110) or tilted magnetic easy axis on STO (001)[26, 27]. Integrating into MTJs allows for PMA stacks using only three layers with the ability to tune the magnetic easy axis. This presents SRO as an important material for MTJs, despite its relatively low Curie temperature. Besides PMA, a sizable TMR is also an important ingredient for wider technological applicability. So far, however, the works that have utilized SRO as ferromagnetic electrodes in MTJs have found relatively low TMR ratios and spin polarization values ranging from -9%[28] to 9.5%[29], and only in-plane transport measurements were reported.

Here we tailor magnetic anisotropy and optimize mul-

tilayer stacks with magnetically decoupled layer for TMR studies. We observe a large TMR ratio in SRO/STO/SRO (001) tunnel junctions of 25% at 10 K. This value is higher than expected when considering only the tunneling spin polarization of the DOS of the electrodes at E_F . Using density functional theory (DFT) calculations we find that transmission in the antiparallel state is significantly reduced over the entire Brillouin zone due to a symmetry mismatch between the propagating Bloch states of the minority and majority spin bands of SRO (001). This theoretical prediction explains our experiential observations, showing that the transmission in the parallel state is significantly larger than the transmission in the antiparallel state, giving rise to a large TMR ratio. Uniquely we also study the angular variation of the TMR which reveals that the electrodes contain multiple magnetic domains with strong perpendicular magnetic anisotropy, allowing the devices to exhibit at least three stable resistance states. Overall the use of SRO in MTJs provides a facile method for achieving perpendicular magnetic anisotropy and a sizable TMR ratio for potential applications in emerging technologies beyond conventional MRAMs such as in new energy-efficient computing hardware.

SRO (28.8 nm)/STO (4.7 nm)/SRO (51.5 nm) epitaxial trilayer structures are grown on single crystal (001)-

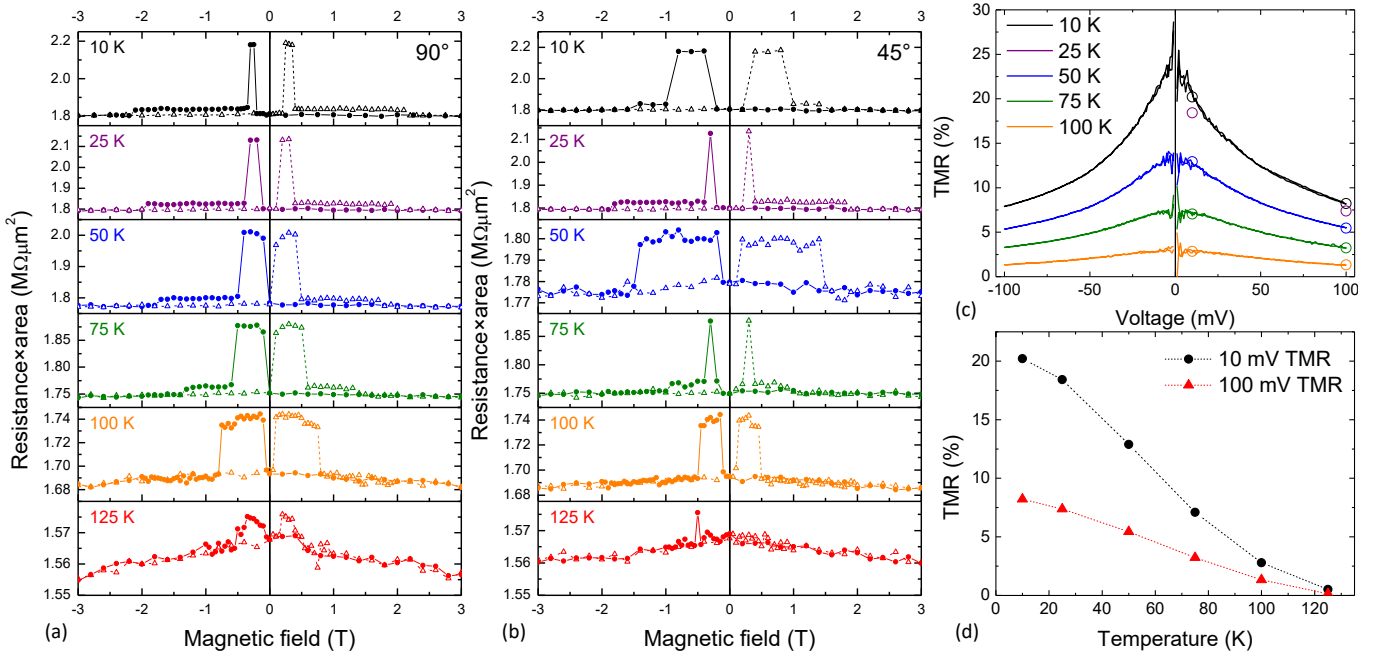


FIG. 2. Resistance-area product versus magnetic field at various temperature with the field applied (a) out-of-plane and (b) along 45° . From top to bottom, the temperatures are 10 K (black), 25 K (purple), 50 K (blue), 75 K (green), 100 K (orange) and 125 K (red). The applied voltage is 10 mV and the field is swept from $+5$ T to -5 T (solid circles) and -5 T to $+5$ T (empty triangles). (c) Bias dependence of tunneling magnetoresistance (TMR) percentage at different temperatures. The lines are extracted from voltage sweeps with the field out-of-plane, and the open circles are based on the field sweeps. (d) Temperature dependence of TMR at 10 mV (black circles) and 100 mV (red triangles).

oriented STO substrates by pulsed laser deposition[30]. X-ray diffraction data (Fig. 1(a) and Supplemental Material Fig. S1) show that the SRO in-plane lattice parameters match those of STO, indicating the orientation of the SRO unit cell adopts that of the STO substrate and the heterostructure is fully strained. Along the out-of-plane direction, the SRO unit cell exhibits a small tensile strain of around 0.5%, consistent with earlier reports[21, 27].

Atomic force microscopy images of the grown films demonstrate the films grew by step bunching, shown in Fig. 1(b). This growth mode is commonly observed in SRO films grown on vicinal STO surfaces when the terrace width is high and the flux is relatively low[31] or when the film thickness surpasses a critical thickness[32–34].

Field-cooled magnetization-temperature (M-T) measurements are performed while applying a 6.5 T magnetic field along different directions. Figure 1(c) shows Curie-Weiss behavior in all directions with a Curie temperature of around 140 K. Magnetization versus magnetic field loops are shown in Figs. 1(d) and (e) for 10 K and 100 K, respectively. Figure 1(d) demonstrates a significant loop opening in all directions. The coercivity is largest when the field is applied along the film normal and smallest with the field applied in-plane. Step-like features appear in the loops, indicating that the two SRO layers are mag-

netically decoupled and switching independently. These results indicate that the magnetic easy axis lies close to the film normal but is slightly tilted towards the film plane.

After performing structural and magnetic measurements, the layer stacks are patterned into elliptical MTJs using UV lithography and standard device fabrication[30]. The resistance of the bottom electrode shows metallic behavior and increases with temperature from $120\ \Omega$ at 10 K to $190\ \Omega$ at 100 K (Supplemental Material Fig. S2). The tunnel junction resistance, on the other hand, decreases with temperature and is around two orders of magnitude higher ranging from $11.5\ k\Omega$ at 10 K to $10.8\ k\Omega$ at 100 K. Resistance versus magnetic field measurements are conducted with the field applied along different directions. By applying the field along different directions we are able to study the temperature dependence of the anisotropy on an individual layer in the device. Figures 2(a) and (b) show the resistance \times area versus magnetic field curves measured at 10 mV for a $157.1\ \mu\text{m}^2$ junction with the field applied along the film normal and at 45° to the normal. Measurements with the field applied in-plane and with a higher voltage bias can be found in Supplemental Material Figs S3 and S4. The TMR ratio is defined as:

$$TMR = \frac{\Delta R}{R_P} = \frac{R_{AP} - R_P}{R_P}, \quad (1)$$

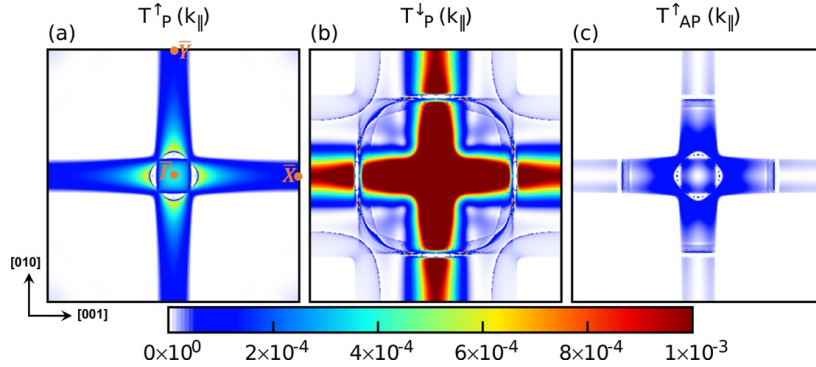


FIG. 3. Transmission of the $\text{SrRuO}_3/\text{SrTiO}_3/\text{SrRuO}_3$ MTJ. k_{\parallel} -resolved transmission in the 2D Brillouin zone at the Fermi energy (E_F) for (a) majority- and (b) minority-spin electrons for parallel magnetization of the SRO electrodes and (c) majority(minority)-spin electrons for antiparallel magnetization.

where the resistances of the junction in the antiparallel and parallel states are R_{AP} and R_P , respectively. The dependences of the TMR ratio on voltage bias and temperature are summarized in Figs 2(c) and (d).

At 10 K with the field applied along the surface normal (90°), three regimes are observed. At high fields, both layers are aligned in the field direction giving rise to a parallel state with low resistance. When the field is reversed, a large increase in the resistance ensues indicating that the antiparallel state is reached. This state persists for a small field range after which the resistance decreases to an intermediate state indicating that a domain in the opposite electrode is reversed. This state is maintained for a relatively large field range after which the rest of the layer switches giving rise to the parallel state. Similarly, when the field is applied 45° to the normal, three regions are seen; in this case, however, the high resistance antiparallel state persists for a larger field range. With increasing temperature, the switching field of the intermediate regime decreases. The field range spanning the antiparallel state, on the other hand, increases in the normal direction and decreases at 45° . From these results, it is clear that switching occurs through a multidomain configuration and that the anisotropy is greatly influenced by temperature. It is well established that the magnetocrystalline anisotropy of SRO is strongly temperature-dependent: it has been demonstrated that the anisotropy constants are dependent on temperature[35] and that the anisotropy axes exhibit a complex symmetry that changes as a function of temperature[36].

Here, the existence of multiple domains with strong perpendicular components is consistent with the field sweeps in all directions. Supplemental Material Figs S3-S5 show that it is energetically unfavourable for the magnetization to lie in-plane. When the field is applied normally or at 45° to the film, the switch from antiparallel to parallel occurs in two steps, characteristic of domains with different coercivities reversing at distinct fields. If

the field is applied in-plane, on the other hand, the magnetization is pulled out-of-plane when the field is sufficiently weak in localized regions. The bias dependence of the TMR can be related to the bias dependence of the electronic structure of SRO/STO interface and will also be influenced by spin-wave excitations by tunneling electrons across this interface[37-40].

At 10 K we find a maximum TMR of 25%, which corresponds to a tunnel spin polarization magnitude of $\pm 33\%$ according to the Jullière model[41]. Due to the symmetric nature of the MTJ stack the sign of the spin polarization cannot be determined. This value is higher than the previous experimental demonstrations of -9% and -9.5% reported in Ref. [28] and [29] respectively with an STO tunnel barrier, and the theoretical spin polarization determined from the density of states [42-44]. Hence, this high TMR ratio cannot be explained by the conventional model and we should consider the specific aspects of the evanescent states relevant here, by considering the role of symmetry and spin.

To gain a microscopic understanding of the origin of the TMR in the SRO-based MTJs, we carry out conductance calculations using the non-equilibrium Green's function formalism[30]. We first calculate the number of spin- and momentum-dependent conduction channels, i.e. the number of propagating Bloch states in the momentum space in the SRO (001) electrodes, that is determined by

$$N_{\parallel}^{\sigma}(\vec{k}_{\parallel}) = \frac{\hbar}{2} \sum_n \int |v_{nz}^{\sigma}| \frac{\partial f}{\partial E_n^{\sigma}(\vec{k})} dk_z, \quad (2)$$

where σ denotes the spin index (\uparrow or \downarrow), \vec{k} is the wave vector in the three-dimensional Brillouin zone, $\vec{k}_{\parallel} = (k_x, k_y)$ is the transverse wave vector, E_n^{σ} is energy of band n , $v_{nz}^{\sigma} = \frac{1}{\hbar} \frac{\partial E_n^{\sigma}(\vec{k})}{\partial k_z}$ is the band velocity along the transport z direction, and f is the Fermi distribution function. Supplemental Material Figs S7 (a) and (b) show the distribution of conduction channels at

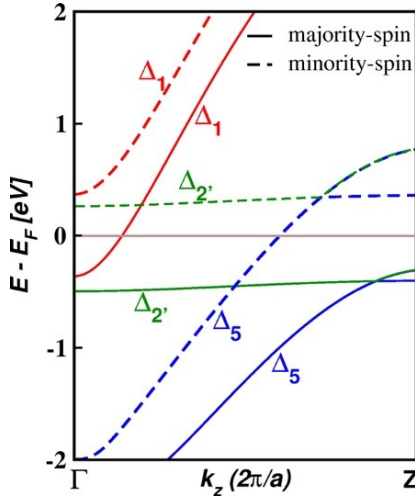


FIG. 4. Electronic band structure of SrRuO_3 : Spin-polarized bands along the [001] direction for SrRuO_3 . Majority-spin (solid) and minority-spin (dashed) bands near the Fermi energy are labeled with their symmetry. The Fermi energy is set to zero (brown line).

E_F reflecting the projection of the Fermi surface of bulk SRO to the (001) plane. From the distribution of N_{\parallel}^{\uparrow} and $N_{\parallel}^{\downarrow}$ in the two-dimensional (2D) Brillouin zone of SRO (001), we obtain a \vec{k}_{\parallel} -dependent spin polarization $p_{\parallel}(\vec{k}_{\parallel}) = \frac{N_{\parallel}^{\uparrow} - N_{\parallel}^{\downarrow}}{N_{\parallel}^{\uparrow} + N_{\parallel}^{\downarrow}}$ (Supplemental Material Fig. S7(c)) and find a net spin polarization $p = \frac{\sum N_{\parallel}^{\uparrow} - \sum N_{\parallel}^{\downarrow}}{\sum N_{\parallel}^{\uparrow} + \sum N_{\parallel}^{\downarrow}}$ of about -57%.

Then we calculate the conductance of an SRO/STO/SRO (001) MTJ, by connecting the optimized SRO/STO/SRO (001) heterostructure to two semi-infinite SRO (001) electrodes. Figures 3(a),(b) and (c) show the calculated \vec{k}_{\parallel} -resolved transmission at the Fermi energy for the parallel (P) magnetization of two electrodes, $T_P^{\sigma}(\vec{k}_{\parallel})$, and for the antiparallel (AP) magnetization of two electrodes, $T_{AP}^{\sigma}(\vec{k}_{\parallel})$, where the $\sigma = \uparrow$ or \downarrow is the spin index. Note that $T_{AP}^{\uparrow}(\vec{k}_{\parallel}) = T_{AP}^{\downarrow}(\vec{k}_{\parallel})$ by symmetry.

As is evident from Fig. 3, transmission for the AP state is strongly reduced compared to transmission for the P state. To gain insight into the observed large changes in the distribution of $T^{\sigma}(\vec{k}_{\parallel})$ for P and AP states, we analyze the symmetry of the tunneling Bloch states in SRO (001) and of the evanescent states in STO (001). In bulk SRO and STO, the cubic crystal field of oxygen octahedra splits the d -orbitals of Ru and Ti atoms into a higher energy level of two-fold degenerate e_g (d_{z^2} , $d_{x^2-y^2}$) bands and a lower energy level of three-fold degenerate t_{2g} (d_{xy} , d_{xz} , d_{yz}) bands. In an SRO/STO/SRO (001) MTJ, the symmetry is lowered from cubic to tetrag-

onal thus lifting the partial degeneracy of the t_{2g} and e_g bands: the t_{2g} band splits into a doubly degenerate (d_{xz} , d_{yz}) band and a non-degenerate d_{xy} band while the e_g band splits into non-degenerate d_{z^2} and $d_{x^2-y^2}$ bands. Thus, along the [001] direction of the layered perovskite structure, the symmetry group of the wave vector is equivalent to that of the C_{4v} point group and has four irreducible representations: $\Delta_5(xz, yz)$, $\Delta_2(xy)$, $\Delta_1(z^2)$, and $\Delta'_2(x^2 - y^2)$. Figure 4 shows the band structure of SRO along the $\Gamma - Z$ symmetry line, indicating that there are three bands crossing the Fermi energy: the majority-spin band of Δ_1 symmetry and doubly degenerate minority-spin bands of Δ_5 symmetry.

To be efficiently transmitted across the STO barrier layer, the symmetry of these propagating Bloch states in SRO (001) has to match the symmetry of low-decay-rate evanescent states in STO (001). The evanescent states appear within the band gap of STO and represent its wave functions that decay exponentially with a rate κ , determined by the complex band structure. Along the [001] direction, the complex bands with the lowest decay rates represent a Δ_5 doublet and a Δ_1 singlet (Supplemental Material Fig. S8(a)). The wave-function symmetry must be maintained across the whole crystalline MTJ. As a result, for the P-aligned MTJ, the Γ point majority-spin states of SRO decay inside the barrier according to the Δ_1 band of STO, whereas the minority-spin states of SRO decay according to the Δ_5 band, giving rise a perfect correspondence between symmetry and spin. In contrast, for the AP-aligned MTJ, majority-spin Δ_1 states of the left electrode cannot be transmitted to the minority-spin Δ_5 states of the right electrode and vice versa. Thus, the transmission of the AP-aligned MTJ is zero at the Γ point and significantly reduced in the whole 2D Brillouin zone due to this symmetry mismatch (Fig. 3(c)). As a result, the transmission in the parallel state is significantly larger than the transmission in the antiparallel state.

To obtain the TMR value we calculate the total transmission for the parallel (T_P) and antiparallel (T_{AP}) states by integrating $T_{\sigma}(\vec{k}_{\parallel})$ over \vec{k}_{\parallel} and σ . T_P is found to be significantly greater than T_{AP} , leading to a giant TMR ratio $\frac{T_P - T_{AP}}{T_{AP}}$ of 1800%. This calculated TMR ratio is larger than the experimentally measured value. This discrepancy could be due to various factors that are not considered in the theoretical calculations. One of the main factors is likely imperfections of the STO barrier layer (e.g., oxygen vacancies) which may lead to the diffuse scattering of the transmitted waves breaking \vec{k}_{\parallel} conservation and thus the symmetry rules. Among other factors are

- (i) orthorhombic distortions of the RuO_6 octahedra;
- (ii) imperfections of the interfaces which may lead to non-collinear and loose spins;

(iii) effect of spin-orbit coupling (which is large in SRO) mixing the spin channels;

The strong spin-orbit coupling of the heavy Ru ions in SRO gives rise to its magnetocrystalline anisotropy, which can be exploited to overcome technical challenges related to creating optimized MTJ stack with two ferromagnetic electrodes with PMA. We demonstrate that the magnetization of both layers lies out-of-plane with a minimal number of layers and that these layers can be made to switch independently while still permitting tunneling when an STO barrier is inserted. The angle-dependent TMR measurements show that the anisotropy is complex and has an out-of-plane component and a strong temperature dependence.

For technologically viable MTJs, PMA and current-controlled switching of the magnetization are desired along with a sizable TMR. This can be achieved through spin-orbit torque, but in a system with perfect PMA the symmetry has to be broken to achieve deterministic switching. This can be intrinsically achieved by slightly tilting the magnetic easy axis. Alternatively, a perfectly out-of-plane easy axis gives rise to probabilistic switching[26, 27]. Hence, the use of SRO could provide a way to break the symmetry and achieve deterministic field-free current-induced switching or realize probabilistic switching, which can be used for p-bits.

In summary, we investigated all-oxide magnetic tunnel junctions with out-of-plane magnetic axes controlled by the substrate. We showed a sizable TMR of 25% and multiple states at 10 K, significantly larger than previous measurements in SRO/STO/SRO MTJs and larger than what can be understood from the theoretical spin polarization of SRO. Using density functional theory (DFT) calculations we determined that the TMR is enhanced by differences in the decay symmetry exhibited by the majority- and minority-spin states of SRO in the barrier. This perfect correspondence between symmetry and spin explains our experiential data. For practical applications both PMA and a significant TMR ratio are important. Additionally, our results demonstrate that the complex and temperature-dependent anisotropy of SRO is reflected in changes in TMR, indicating that TMR can be utilized to study magnetic anisotropy on an individual layer in the device.

Schilfgaarde, S. S. Jaswal, and E. Y. Tsymbal, *Phys. Rev. Lett.* **95**, 216601 (2005).

[5] J. M. De Teresa, A. Barthélémy, A. Fert, J. P. Contour, F. Montaigne, and P. Seneor, *Science* **286**, 507 (1999).

[6] J. De Teresa, A. Barthélémy, A. Fert, J. Contour, R. Lyonnet, F. Montaigne, P. Seneor, and A. Vaures, *Physical Review Letters* **82**, 4288 (1999).

[7] S. Yuasa, T. Nagahama, A. Fukushima, Y. Suzuki, and K. Ando, *Nature Materials* **3**, 868 (2004); S. S. P. Parkin, C. Kaiser, A. Panchula, P. M. Rice, B. Hughes, M. Samant, and S.-H. Yang, *ibid.* **3**, 862 (2004).

[8] S. Ikeda, K. Miura, H. Yamamoto, K. Mizunuma, H. Gan, M. Endo, S. Kanai, J. Hayakawa, F. Matsukura, and H. Ohno, *Nature materials* **9**, 721 (2010).

[9] T. Scheike, Z. Wen, H. Sukegawa, and S. Mitani, *Applied Physics Letters* **122** (2023).

[10] J. Torrejon, M. Riou, F. A. Araujo, S. Tsunegi, G. Khalsa, D. Querlioz, P. Bortolotti, V. Cros, K. Yakushiji, A. Fukushima, *et al.*, *Nature* **547**, 428 (2017).

[11] W. A. Borders, A. Z. Pervaiz, S. Fukami, K. Y. Camsari, H. Ohno, and S. Datta, *Nature* **573**, 390 (2019).

[12] K. Y. Camsari, B. M. Sutton, and S. Datta, *Applied Physics Reviews* **6**, 011305 (2019).

[13] M. Bowen, M. Bibes, A. Barthélémy, J.-P. Contour, A. Anane, Y. Lemaitre, and A. Fert, *Applied Physics Letters* **82**, 233 (2003).

[14] J. P. Velev, C.-G. Duan, J. Burton, A. Smogunov, M. K. Niranjan, E. Tosatti, S. Jaswal, and E. Y. Tsymbal, *Nano letters* **9**, 427 (2009).

[15] S. Ikeda, H. Sato, H. Honjo, E. Enobio, S. Ishikawa, M. Yamanouchi, S. Fukami, S. Kanai, F. Matsukura, T. Endoh, *et al.*, in *2014 IEEE International Electron Devices Meeting* (IEEE, 2014) pp. 33–2.

[16] M. Wang, Y. Zhang, X. Zhao, and W. Zhao, *Micromachines* **6**, 1023 (2015).

[17] A. Kanbayasi, *Journal of the physical society of japan* **41**, 1876 (1976).

[18] A. Callaghan, C. W. Moeller, and R. Ward, *Inorganic Chemistry* **5**, 1572 (1966).

[19] Y. Chen, D. Bergman, and A. Burkov, *Physical Review B* **88**, 125110 (2013).

[20] S. Itoh, Y. Endoh, T. Yokoo, S. Ibuka, J.-G. Park, Y. Kaneko, K. S. Takahashi, Y. Tokura, and N. Nagaosa, *Nature Communications* **7**, 11788 (2016).

[21] P. Zhang, A. Das, E. Barts, M. Azhar, L. Si, K. Held, M. Mostovoy, and T. Banerjee, *Physical Review Research* **2**, 032026 (2020).

[22] K. Takiguchi, Y. K. Wakabayashi, H. Irie, Y. Krockenberger, T. Otsuka, H. Sawada, S. A. Nikolaev, H. Das, M. Tanaka, Y. Taniyasu, *et al.*, *Nature communications* **11**, 4969 (2020).

[23] S. Kaneta-Takada, Y. K. Wakabayashi, Y. Krockenberger, S. Ohya, M. Tanaka, Y. Taniyasu, and H. Yamamoto, *Applied Physics Letters* **118**, 092408 (2021).

[24] P. Zhang, A. Das, J. van Rijn, A. Watson, and T. Banerjee, *Applied Physics Letters* **121** (2022).

[25] Y. Gu, Q. Wang, W. Hu, W. Liu, Z. Zhang, F. Pan, and C. Song, *Journal of Physics D: Applied Physics* **55**, 233001 (2022).

[26] L. Liu, Q. Qin, W. Lin, C. Li, Q. Xie, S. He, X. Shu, C. Zhou, Z. Lim, J. Yu, W. Lu, M. Li, X. Yan, S. J. Pennycook, and J. Chen, *Nature Nanotechnology* **14**, 939 (2019).

* t.banerjee@rug.nl

[1] W. Butler, X.-G. Zhang, T. Schulthess, and J. MacLaren, *Physical Review B* **63**, 054416 (2001).

[2] P. LeClair, J. Kohlhepp, H. Swagten, and W. de Jonge, *Physical Review Letters* **86**, 1066 (2001).

[3] K. D. Belashchenko, E. Y. Tsymbal, M. van Schilfgaarde, D. A. Stewart, I. I. Oleynik, and S. S. Jaswal, *Phys. Rev. B* **69**, 174408 (2004).

[4] J. P. Velev, K. D. Belashchenko, D. A. Stewart, M. van

- [27] A. S. Goossens, M. A. T. Leiviskä, and T. Banerjee, *Frontiers in Nanotechnology* **3**, 680468 (2021).
- [28] J. Noh, C. Eom, M. Lagally, J. Sun, and H. Kim, *physica status solidi (b)* **241**, 1490 (2004).
- [29] D. Worledge and T. Geballe, *Physical Review Letters* **85**, 5182 (2000).
- [30] See Supplemental Information at [URL will be inserted by publisher] for further details on the growth, fabrication and theoretical methods.
- [31] W. Hong, H. N. Lee, M. Yoon, H. M. Christen, D. H. Lowndes, Z. Suo, and Z. Zhang, *Physical Review Letters* **95**, 1 (2005).
- [32] M. Yoon, H. N. Lee, W. Hong, H. M. Christen, Z. Zhang, and Z. Suo, *Physical Review Letters* **99**, 1 (2007).
- [33] D. Estève, T. Maroutian, V. Pillard, and P. Lecoeur, *Physical Review B* **83**, 193401 (2011).
- [34] A. Gura, G. Bertino, B. Bein, and M. Dawber, *Applied Physics Letters* **112**, 1 (2018).
- [35] A. Kanbayasi, *Journal of the Physical Society of Japan* **41**, 1879 (1976).
- [36] M. Ziese, I. Vrejoiu, and D. Hesse, *Physical Review B - Condensed Matter and Materials Physics* **81**, 1 (2010).
- [37] S. Zhang, P. Levy, A. Marley, and S. Parkin, *Physical Review Letters* **79**, 3744 (1997).
- [38] J. S. Moodera, J. Nowak, and R. J. van de Veerdonk, *Physical Review Letters* **80**, 2941 (1998).
- [39] B. G. Park, T. Banerjee, B. Min, J. G. Sanderink, J. Lodder, and R. Jansen, *Journal of Applied Physics* **98** (2005).
- [40] B. G. Park, T. Banerjee, J. Lodder, and R. Jansen, *Physical Review Letters* **99**, 217206 (2007).
- [41] M. Jullière, *Physics Letters A* **54**, 225 (1975).
- [42] P. Allen, H. Berger, O. Chauvet, L. Forro, T. Jarlborg, A. Junod, B. Revaz, and G. Santi, *Physical Review B* **53**, 4393 (1996).
- [43] D. J. Singh, *Journal of Applied Physics* **79**, 4818 (1996).
- [44] I. Mazin and D. J. Singh, *Physical Review B* **56**, 2556 (1997).